Effects of multiple loads in a contactless, inductively coupled linear power transfer system

Derk Wesemann[1], Stefan Witte[1], and Jan-Stefan Michels[2]

[1]inIT - Institute Industrial IT, OWL University of Applied Sciences, D-32657 Lemgo, Germany
derk.wesemann@hs-owl.de, stefan.witte@hs-owl.de
[2]Weidmüller Interface GmbH & Co. KG, D-32758 Detmold, Germany
janstefan.michels@weidmueller.de

Abstract

This paper describes an approach for a contactless, inductively coupled resonant energy supply system for multiple, independent endpoints. Typical contactless inductive energy supplies in industrial applications involve a combination of one primary inverter/coil and one secondary coil with a rectifier and a load. The work presented in this paper issues a one-to-many-approach instead, which can be used for creating a contactless automation network, having multiple secondary side loads driven by only one primary coil. The challenge is to run such a system in resonance, as every participant potentially affects the resonant frequency, and therefore the overall system efficiency. The effects of multiple participants on the resonant frequency are modeled, and the theoretical examinations are backed up by measurements run on a rail-based test system.

1. Introduction

Contactless energy transfer has become a major issue in modern automation scenarios, as it offers reduced installation efforts, more flexibility and movability together with an elimination of wear and tear of supply cables. Current research focuses on an inductive power supply of a single load over a possibly large distance [1], or for charging purposes of mobile installations and vehicles [2].

Another area of high power applications is in the rail-based supply of large moving loads, within the kilowatt-range. The work that has been carried out in this direction is most often referred to as the sliding transformer [3], [4]. The other end of the power supply level scale is marked by the RFID technology, where only very small amounts of energy are needed to power an RFID tag. In RFID applications, there is also a first introduction of multiple secondary sides, but their effect on the power efficiency is not considered relevant for the application. Attempts for achieving a supply of multiple loads lead in the direction of a cable-based solution [5].

This work aims for creating an energy supply system for a modular system of a large number of devices aligned on one solid installation rail. The devices should be able to function at any place on the rail, delivering an output power of up to 10W each. The application does not demand to have them moved along the rail while in use, which allows a very small and almost invariable coupling distance and a high coupling factor, compared to the common research aims of transcending a possibly large distance. For the rail dimensions, a length of 1m was given together with a width of 24mm. An E-shaped ferromagnetic core was embedded into the rail to allow a well-guided magnetic field and to minimize the stray losses due to metalized material in the surroundings.

It is necessary to describe the change in resonant frequency depending on the number of secondary side loads, as well as the transducer efficiency, as it is affected by the number and value of loads. All subsequent work was carried out with these (application specific) premises:

- Primary supply rail setup with E-shaped core material cross section.
- Secondary side with identical E-core.
- Constant distance between every secondary and the primary side.
- Constant mutual inductance for every single transducer element.

2. Problem description

Compared to common transformers, the geometrical layout of contactless inductive power transfer system (CIPT) for multiple secondary side loads provides some disadvantages. While the coupling coefficient k of a conventional transformer is typically very high ($k \rightarrow 1$), representing a very small stray field, the effective coupling coefficient for the contactless transformer dramatically decreases. This effect is partly based on the coupling distance, but also due to the large primary coil area and the comparably small secondary pickups, implying a considerable large stray field.

The general system description of an inductive energy transfer to multiple loads as it is shown in figure 1 can be described by a transducer having multiple secondary sides. This transducer is driven by an inverter, which creates an AC signal of the desired operating frequency. The inverter itself takes a DC input, which is delivered by an appropriate rectifier from a typical AC supply like 230 or 400V. On the secondary side, a rectifier followed by a DC/DC-Converter is used to generate the desired output voltage to drive the secondary side loads.

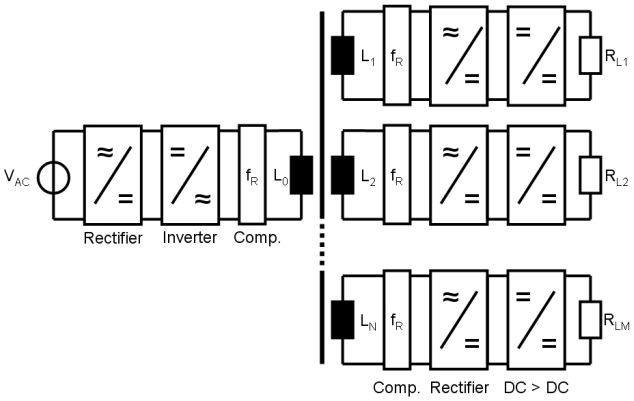

Fig. 1. System description

For handling small coupling factors, it is essential to minimizing the inductive losses introduced by the large stray inductances, which can be performed by applying a compensation circuit. This circuit typically has the form of a serial or parallel resonant circuitry, using a capacitance to compensate for the phase delay, which is introduced by the inductance of the transducer coils. Since it is possible to arrange this resonant capacitance in a serial or parallel way, different compensation modes can be realized:

- Serial-Serial compensation
- Serial-Parallel compensation
- Parallel-Serial compensation
- Parallel-Parallel compensation

In conventional transformer scenarios containing one primary and one secondary side only, the compensation mode leads to a constant operating frequency. In a system with multiple secondary sides which are attached using ferrite cores, like it is the case in the given application, each secondary side directly affects the inductance of the primary coil, leading to a change in the overall system resonant frequency. This change has to be compensated by either tuning the operating frequency of the power inverter or by adjusting the value of the resonant capacitance, according to the number of participants.

3. Multiple pick-up system

To be able to predict the change of inductance and react appropriately, it is necessary to describe the relation between the primary inductance L_P and the number of participants M mathematically. This work proposes an approach which is based on geometrically dividing the primary coil in areas which are occupied by secondary sides (participants) and unoccupied (free) areas, which contribute to the stray field only. The overall primary inductance can then be calculated by taking the sum of the stray inductance L_0 and the primary coupling inductance L_{PM}.

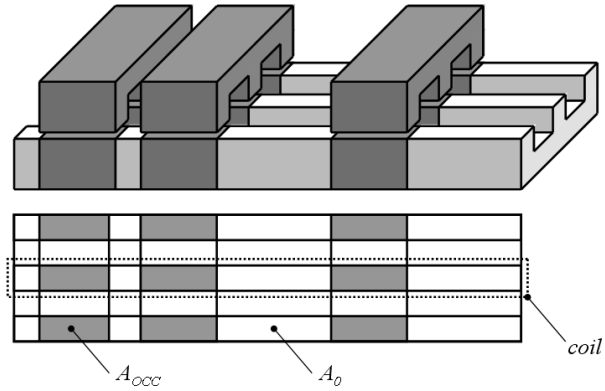

Fig. 2. Area distribution of occupied and unoccupied positions

The rail can be divided into occupied (A_{OCC}) and unoccupied (A_0) areas, each one contributing to the overall primary inductance, for the primary coil winding encloses the center beam of the E-core. The difference in magnetic path length, effective area and material permeability between the two different position properties results in different magnetic reluctances, respectively inductances. These inductances can together be regarded as being connected in a serial circuit, and therefore the overall inductance value is to be calculated by taking the sum of all fragment inductances L_{PM} (appearing at any occupied position A_{OCC}) and the stray inductance $L_{0\sigma}$ (defined by the effective free area A_0).

$$L_P = L_{0\sigma} + M \cdot L_{PM} \qquad (1)$$

For the two different position properties, the following theoretical models are used to calculate the particular inductance.

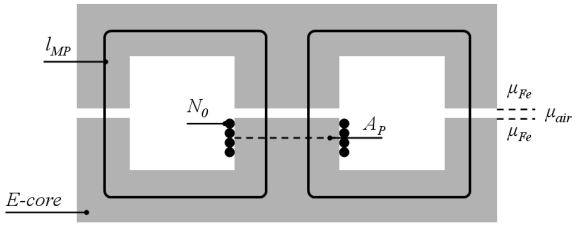

Fig. 3a. Occupied rail position

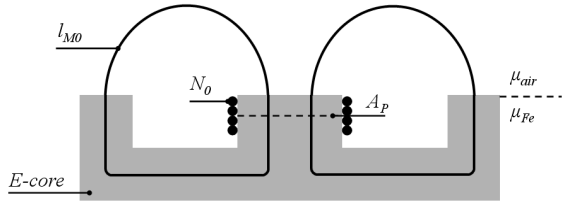

Fig. 3b. Free rail position

The two properties differ in means of the magnetic path length l_M (l_{MP}, l_{M0}), the magnetic field medium (characterized by the permeabilities μ_{air}, μ_{FE}) and the resulting magnetic reluctance R_M. The inductance of each area can be expressed as

the product of the reciprocal reluctance and the number of primary coil windings *N*.

$$L_{PM} = \frac{\mu_{effP} \cdot N_0^{\,2} \cdot A_{OCC}}{l_{MP}} \qquad (2)$$

The magnetic path length l_{MP} is approximated from the geometric layout auf the E-core. N_0 equals the number of windings of the primary coil. The stray inductance $L_{0\sigma}$ is depending on the geometry of the system. Any magnetic field line which does refer to a current flowing through the primary coil and which is not passing through the secondary coil contributes to the stray inductance. In a system with a variable secondary side number but a constant primary coil size, like it is the case in the proposed application, the value of the stray inductance is also depending on the occupation status of the system. This relation can be illustrated by taking a closer look on having either one participant attached to the network or the maximum number of participants. Having only one secondary side, the effective area for the stray inductance which is defined by the primary coil area is considerably large, leading to a high stray inductance. With the maximum number of participants, the effective area for the stray inductance decreases, together with its value. Generally, the variable stray inductance $L_{0\sigma}$ can be described as:

$$L_{0\sigma} = \frac{\mu_{eff\,0} \cdot N_0^{\,2} \cdot A_0}{l_{M\,0}} \qquad (3)$$

The winding count N_0 is mandatorily identical with the value in (2), but the magnetic path length l_{M0} is different, for the magnetic field lines now are only partly guided by the core material. The effective area A_0 is depending on the number of attached nodes in the following way:

$$A_0 = w_P \cdot \left(l_P - M \cdot l_S\right) \qquad (4)$$

with w_P being the primary coil width, l_P being the total primary coil length, l_S being the length of one secondary side coil and *M* being the number of participants. An additional - but comparably smaller - component for the stray inductance is introduced by the distance between the primary and the secondary coil, which allow part of the magnetic field lines to form a closed loop before passing through the secondary coil area. As the application uses the same core material for both the primary and the secondary side, this part of the stray inductance can be considered to be constant and of equal value for both sides: $L_{\sigma P} = L_{\sigma S}$. With zero distance (direct contact) between the two cores, these two stray inductances will be considered also limiting to zero, as they are small compared to the stray inductance introduced by the large primary coil.

From the given geometry of the primary and secondary coil and the core shape, the inductance values were calculated and compared to the measurements. Typically, the field line distribution requires a complex integral solution which can be achieved with an FEM simulation. The calculations for this work have shown, that for the reluctance contribution of the paths within the core material, a geometrical approximation for the average path length leads to sufficiently accurate results, while the greatest source for errors is to be found in the distance of the air gap between two E-cores at the occupied positions.

For the magnetic field lines within the core material, the average field line length was approximated by choosing the center path in each core segment. The result of this approximation is accurate within 15% compared to the value given by the core manufacturer.

The approximation for the field lines spanning the large air gap at an unoccupied position is even coarser, for calculation simplification the average path shape was presumed to have a circular appearance. Both path shapes are depicted in figure 3a and 3b, respectively. An equivalent magnetic circuit can be derived in the following way:

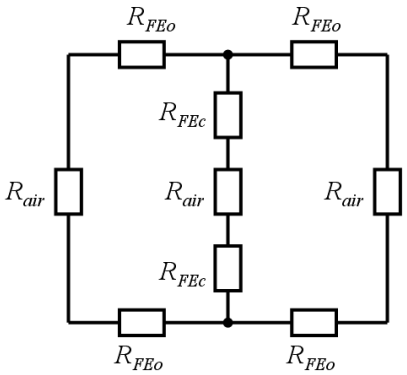

Fig. 4a. Magnetic equivalent circuit, occupied rail

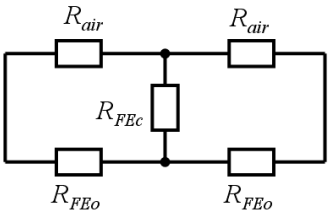

Fig. 4b. Magnetic equivalent circuit, free rail

With an example of having a primary coil with 1 winding and up to 50 participants on the rail, calculation and measurement of the primary coil inductance show the behavior which is illustrated in figure no. 5. Table 1 contains the applications geometrical and material properties.

Table 1. Setup parameters

Parameter	**Value**
core center beam width w_P	4 mm
core outer beam width w_O	2 mm
secondary side element length l_S	10 mm
overall rail length l_P	1 m
core permeability μ_R	1270
air gap magnetic path length l_{1L}	0.15 mm
half core magnetic path length l_{1FE}	14 mm
free air magnetic path length l_{air}	12.57 mm

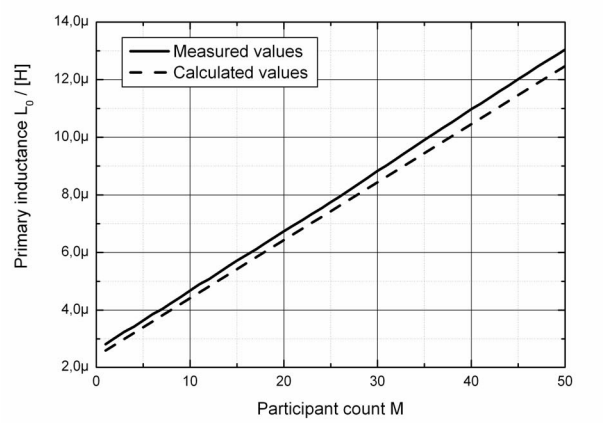

Fig. 5. Primary inductance vs. participant count

The relation between the participant count *M* and the primary inductance shows a linear dependency. A small offset between the calculations and the measurements can be related to the inductance of the supply cables, but basically the calculation model has proven good accuracy compared to the measurements. If the compensating capacitance is kept constant, the resulting resonance frequency drift shows an inverse square-root-behavior, which is illustrated by the measurement results in figure 6:

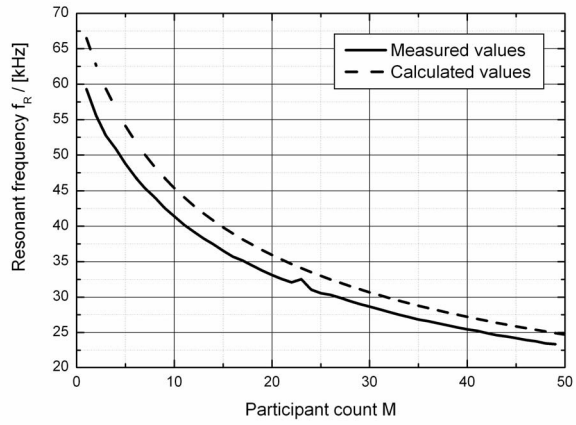

Fig. 6. Measured resonant frequency drift, constant compensation

4. Contactless transformer model

A general contactless transformer model takes into account both the primary and the secondary inductance (L_P, L_S) and the mutual inductance L_M. The current through the primary coil induces a voltage on the secondary side, which is depending on the operating frequency, the mutual inductance and the current strength. This relation works bidirectional, so any current on the secondary side generates an electromagnetic field which is directionally opposed to the stimulating field on the primary side, inducing a voltage on the primary side which is depending on the secondary side current, the mutual inductance and the operating frequency. Including the ohmic losses introduced by the coil windings, this behavioral model and its equivalent circuit is shown in figure no. 7.

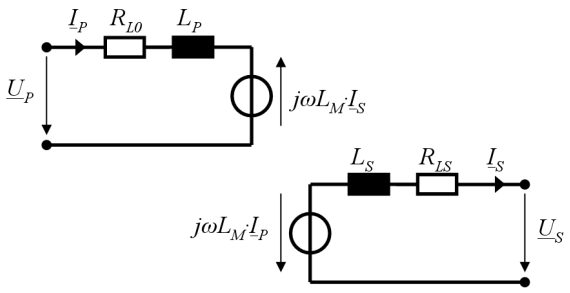

Fig. 7. Equivalent circuit of the lossy transducer

With the compensating capacitance on the secondary side either arranged in parallel or serial circuitry, the secondary side impedance $\underline{Z}_S$ can be expressed as:

Serial compensation:

$$\underline{Z}_{SS} = \frac{1}{j\omega \cdot C_S} + R_{MM} \qquad (5)$$

Parallel compensation:

$$\underline{Z}_{SP} = \frac{1}{j\omega \cdot C_S + \dfrac{1}{R_{MM}}} \qquad (6)$$

with C_S being the resonant capacitance and R_{MM} being the secondary side load, in general. For the primary side, the load on the secondary side is represented by the reflected (or transformed) impedance $\underline{Z}_T$.

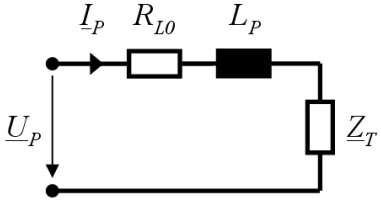

Fig. 8. Simplified equivalent circuit with transformed impedance

The primary input voltage $\underline{U}_P$ drops over the series resistance of R_{L0}, L_P and $\underline{Z}_T$:

$$\underline{U}_P = \left(R_{L0} + j\omega L_P\right) \cdot \underline{I}_P - j\omega L_M \cdot \underline{I}_S \qquad (7)$$

On the secondary side, the current $\underline{I}_S$ can be found in the expression of the voltage loop, including the induced voltage from the primary side:

$$j\omega L_M \cdot \underline{I}_P = \left(R_{LS} + j\omega L_S + \underline{Z}_S\right) \cdot \underline{I}_S$$
$$\Leftrightarrow \underline{I}_S = \frac{j\omega L_M \cdot \underline{I}_P}{R_{LS} + j\omega L_S + \underline{Z}_S} \qquad (8)$$

By inserting the solution for $\underline{I}_S$ of equation no. (8) into (7), the transformed impedance $\underline{Z}_T$ can be extracted as:

$$\underline{Z}_T = \frac{\omega^2 {L_M}^2}{R_{LS} + j\omega L_S + \underline{Z}_S} \qquad (9)$$

From this general form, the expression for multiple (M) secondary loads can be written in the following way, according to figure no. 9:

$$\underline{Z}_T = M \cdot \left(j\omega \cdot L_{PM} + \frac{\omega^2 {L_M}^2}{R_{LS} + j\omega L_S + \underline{Z}_S} \right) \qquad (10)$$

This way, the transposed impedance for any attached node includes the partial, effective primary inductance segment, and the overall impedance seen from the primary side is represented by a serial circuit of M times $\underline{Z}_T$. Depending on the compensation mode, the primary side input power can be expressed as

Serial compensation

$$\underline{S}_{PS} = \left(R_{L0} + j\omega L_{0\sigma} + \frac{1}{j\omega C_P} + \underline{Z}_T \right) \cdot {\underline{I}_P}^2 \qquad (11)$$

Parallel compensation

$$\underline{S}_{PP} = \left(\frac{1}{\frac{1}{R_{L0} + j\omega L_{0\sigma} + \underline{Z}_T} + j\omega C_P} \right) \cdot {\underline{I}_P}^2 \qquad (12)$$

The single secondary side output power is simply given by the product of the load resistance R_{MM} and he square of the load current.

$$\underline{S}_{SS} = \underline{U}_S \cdot \underline{I}_S = R_{MM} \cdot {\underline{I}_S}^2 \qquad (13)$$

The overall system efficiency is described by the term

$$\eta = \frac{\sum \underline{S}_S}{\underline{S}_P} \qquad (14)$$

For simplification, we assume having identical secondary side loads, therefore the participant count M can be introduced to replace the sum expression:

$$\eta = \frac{M \cdot \underline{S}_S}{\underline{S}_P} \qquad (15)$$

With these premises, the according efficiency equations for all four compensation modes can be formulated. Note that according to equation (8), the factor

$\left(\frac{\underline{I}_S}{\underline{I}_P} \right)^2$ can be rewritten as $-\frac{\omega^2 \cdot k^2 \cdot L_P \cdot L_S}{\left(R_{LS} + j\omega L_S + \underline{Z}_S \right)^2}$

Serial-Serial Compensation

$$\eta_{SS} = \frac{M \cdot R_{MM}}{\left(R_{L0} + j\omega L_{0\sigma} + \frac{1}{j\omega C_P} + \underline{Z}_{TS} \right)} \cdot \left(\frac{\underline{I}_S}{\underline{I}_P} \right)^2 \qquad (16)$$

Serial-Parallel Compensation

$$\eta_{SP} = \frac{M \cdot R_{MM}}{\left(R_{L0} + j\omega L_{0\sigma} + \frac{1}{j\omega C_P} + \underline{Z}_{TP} \right)} \cdot \left(\frac{\underline{I}_S}{\underline{I}_P} \right)^2 \qquad (17)$$

Parallel-Serial Compensation

$$\eta_{PS} = M \cdot R_{MM} \cdot \left(\frac{1}{R_{L0} + j\omega L_{0\sigma} + \underline{Z}_{TS}} + j\omega C_P \right) \cdot \left(\frac{\underline{I}_S}{\underline{I}_P} \right)^2 \qquad (18)$$

Parallel-Parallel Compensation

$$\eta_{PP} = M \cdot R_{MM} \cdot \left(\frac{1}{R_{L0} + j\omega L_{0\sigma} + \underline{Z}_{TP}} + j\omega C_P \right) \cdot \left(\frac{\underline{I}_S}{\underline{I}_P} \right)^2 \qquad (19)$$

Taking the serial-serial compensation as an example, the equation can be simplified in case of the optimal choice of capacitances, which compensate for both secondary and primary side inductances.

$$\eta_{SS} = \frac{M \cdot R_{MM}}{R_{L0} + \frac{M \cdot \omega^2 {L_M}^2}{R_{LS} + R_{MM}}} \cdot \frac{\omega^2 \cdot {L_M}^2}{\left(R_{LS} + R_{MM} \right)^2} \qquad (20)$$

This result points out, that the overall efficiency is proportional to the number of participants, the frequency and the mutual inductance, given the assumption that both primary and secondary side can be compensated to show only real impedance values in any case. This state is not likely to be achieved in the real application, but for efficiency optimization, one might try to choose the mutual inductance and the operating frequency as high as possible (with respect to the core material, which losses are not included in the preceding calculations). In case of an optimal compensation, the most severe influence on the system efficiency can be found in the coupling between the primary and the secondary side.

5. Equivalent circuit

Being able to predict the relation between the systems occupation status and the primary inductance value, an equivalent circuit for modeling the overall system can be constructed in the following way:

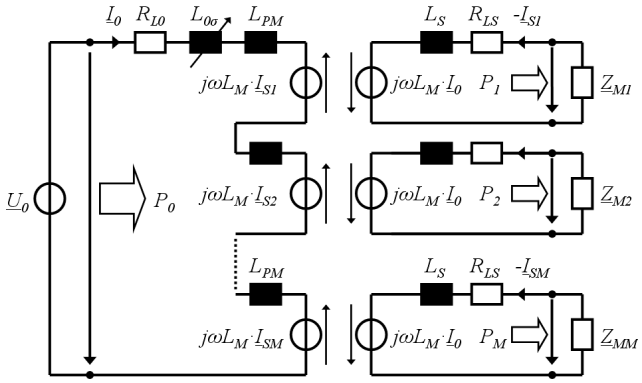

Fig. 9. Equivalent circuit for multiple secondary sides

The ohmic losses of the transducer coils are included in the resistances R_{LS} on the secondary side and R_{L0} on the primary side. These (constant) values are based on the wire diameter, length and material of the coil windings. The mutual inductance is by means of definition related the coupling factor, the value of the primary and the value of the secondary inductance in the following way:

$$k_M = \frac{L_M}{\sqrt{L_{PM} \cdot L_S}} \qquad (21)$$

The coupling factor k_M is based on the partial stray inductances of one occupied rail element only. It can be regarded as constant but also is a purely calculated value, as it can not be measured directly. What can be determined by measurements instead is the overall coupling factor $k < k_M$, which is typically much smaller, due to the larger stray inductance $L_{0\sigma} + M \cdot L_{P\sigma}$.

5. Conclusions

The problems of multiple secondary sides being driven by a common primary coil have been illustrated for the sample application of a rail based contactless inductive power transfer system. A solution for estimating the change in the primary inductance value based on the number of present participants has been modeled and basic calculations for retrieving the system efficiency have been carried out, resulting in an equivalent circuit that is capable of describing the overall system. The test system so far was able to drive a number of 30 loads with a secondary side output power of > 4W each, while the resonant frequency was controlled manually. Further work is going to concentrate on the optimization of the compensation circuitry and the development of a frequency adaptive primary source.

7. References

[1] R. Mecke, C. Rathge, "High frequency resonant inverter for contactless energy transmission over large air gap", IEEE 35th Annual Power Electronics Specialists Conference, Volume 3, 20-25 June 2004, Page(s):1737 - 1743

[2] A. Esser, "Contactless charging and communication for electric vehicles", IEEE Industry Applications Magazine, Volume 1, Issue 6, Nov.-Dec. 1995 Page(s):4 - 11

[3] Wei Xie, Hua Li, Congjiao Wang, "Performance analysis of sliding transformer in contactless inductive power transfer system", International Conference on Electrical Machines and Systems ICEMS, 17-20 Oct. 2008, Page(s):4360 - 4363

[4] Zhang Bingyi, Liu Hongbin, Zhao Yisong, Ying Yong, Feng Guihong, "Contactless electrical energy transmission system using separable transformer", Proceedings of the Eighth International Conference on Electrical Machines and Systems, Volume 3, 29-29 Sept. 2005, Page(s):1721 - 1724

[5] F.F.A. Van der Pijl, J.A. Ferreira, P. Bauer, H. Polinder, "Design of an Inductive Contactless Power System for Multiple Users", Conference Record of the 2006 IEEE Industry Applications Conference, Volume 4, 8-12 Oct. 2006, Page(s):1876 - 1883

[6] J.T. Boys, G.A. Covic, A.W. Green, "Stability and control of inductively coupled power transfer systems", IEE Proceedings in Electric Power Applications, Volume 147, Issue 1, Jan. 2000, Page(s):37 - 43

[7] Chwei-Sen Wang, G.A. Covic, O.H. Stielau, "Power transfer capability and bifurcation phenomena of loosely coupled inductive power transfer systems", IEEE Transactions on Industrial Electronics, Volume 51, Issue 1, Feb. 2004,Page(s):148 -157

[8] Myunghyo Ryu, Honnyong Cha, Yonghwan Park, Juwon Back, "Analysis of the contactless power transfer system using modelling and analysis of the contactless transformer", 31st Annual Conference of IEEE IECON 2005, 6-6 Nov. 2005, Page(s):7 pp.

[9] J. de Boeij, E. Lomonova, J. Duarte, A. Vandenput, "Contactless Energy Transfer to a Moving Actuator", Conference Record of the 2006 IEEE Industry Applications Conference, Volume 4, 8-12 Oct. 2006, Page(s):2020 - 2025

[10] K.W.E. Cheng, Y. Lu, "Development of a contactless power converter", IEEE International Conference on Industrial Technology ICIT, Volume 2, 11-14 Dec. 2002 Page(s):786 - 791